One-dimensional model of the plasma behaviour in Hall effect thrusters

Vittorio Giannetti, Andrea Leporini *, Tommaso Andreussi*, and Mariano Andrenucci**
** University of Pisa.*
Largo Lucio Lazzarino, 1, Pisa, 56121, Italy

Abstract

The typical design process of Hall effect thrusters (HETs) relies on simple scaling rules involving a large set of empirical parameters. For common, SPT-like, configurations, the performance predicted by scaling rules are usually in good agreement with the experimental results. However, the adoption of similar models for different HET configurations is not straightforward and, more often than not, specific experimental campaigns are needed to calibrate the model. In addition, even if a reasonable estimate of the thruster performance can be obtained, it is not possible to address fundamental issues of the thruster behaviour, like the assessment of wall erosion, with simple design rules. In order to bridge this gap the effort to develop a first order HET model is presented in the paper. To obtain a simple and effective model of the plasma behaviour, a quasi-one-dimensional description was used, assuming that the gradients of the plasma properties are dominant in the axial direction. The model allows for an in-depth study of standard HET configurations and includes an accurate description of plasma-wall interactions. The model was then validated against a large set of experimental data for the HT-5k, Sitael's 5kW-class thruster, and for Fakel's SPT-100. The paper presents the comparison between experimental results and model predictions, thus offering a theoretical framework to drive the design of future HETs.

1. Introduction

Hall effect thrusters are electric propulsion devices that are receiving an increasing scientific and technological interest due to their capability of providing high performance coupled with high thrust densities. While a simplified and qualitative discussion on the plasma flow inside the acceleration channel of a Hall effect thruster is a relatively simple task, a clear understanding of the plasma behaviour is an essential factor to improve the HET design and develop new thruster models. This can be achieved only through the development of a reliable physical model and the successive experimental validation of the model predictions. Several models have been proposed, starting from simple one-dimensional models to fully three-dimensional particle-in-cell (PIC) codes. The general trend of the modelization effort is towards 2D hybrid codes: Fife et al. in Ref. [1] presented a 2D hybrid-PIC code, while Mikellides et al., in Ref. [2]-[4], described the Hall2De code and its application, also to non-standard configurations. These numerical codes have the advantage of giving a remarkably detailed representation of the relevant phenomena, together with an accurate description of the physics involved. However, these models are too impenetrable to gain the insight needed to understand the effects of the various parameters on the general thruster operation. Therefore, they lack the capability to give simple design guidelines. On the other hand, Goebel et al. in Ref. [5] presented a simple one-dimensional axial model, whereas Ahedo et al., as reported in Ref. [6]-[8], developed a relatively simple, one-dimensional model of Hall thrusters, that focuses on the sonic transition of the plasma inside the channel. The presence of a sonic point inside the channel, which descends from the fluid description of the plasma, implies the use of a specific, and more complex, integration procedure.

In order to obtain an in-depth insight in the plasma behaviour in the acceleration channel and near plume, we decided to develop a one-dimensional fluid model of the plasma flow. Many significant simplifications were introduced in order to obtain the desired balance between simplicity and reliability of the model, particularly regarding the assumed 1D structure. Keeping all the relevant physics, this first-order model is mainly aimed to rapidly and accurately predict the performance of different thrusters. Once the thruster geometry and main operational parameters are defined, the model can compute the profiles of all the plasma properties in the channel. With the computed plasma properties, the model is also capable of predicting the erosion rate of the channel walls.

The model was used to predict the operation performance of two different thrusters: Sitael's HT5k, a 5kW power class HET, and Fakel's SPT-100, which has a nominal operating power of 1.35 kW. The experimental data collected

for the thrusters were compared to the simulation results, validating the model capability to correctly describe the plasma flow inside the thruster channel.
In Section 2, the one-dimensional model is described in detail. In particular, we analyzed the radial plasma behaviour, the plasma wall-interactions, and the near-plume model. Next, the applied boundary conditions are discussed. Furthermore, the effects of the pressure and of the ion velocity boundary condition on the solution are presented.
In Section 3 and 4 the model results for the HT5k and the SPT-100 are reported. Moreover, model results are compared with experimental data and the trend of the plasma properties and thruster performance is discussed.
Finally, Section 5 presents the conclusions of the work, highlighting the main features and results of the model.

2. Formulation of the Model

The geometrical scheme of a Hall effect thruster is illustrated in Fig. 1. We introduce the cylindrical coordinates (r, θ, z) and we assumed $z = 0$ at the anode surface. The channel exit is at $z = L_{ch}$ and the cathode is placed at a distance L_{cat} from the anode. The domain ranges axially from the anode to the cathode, whereas in the radial direction the plasma is bounded by the inner and outer ceramic walls. Outside the acceleration channel, in the plume region, the plasma is free to expand in the radial direction.

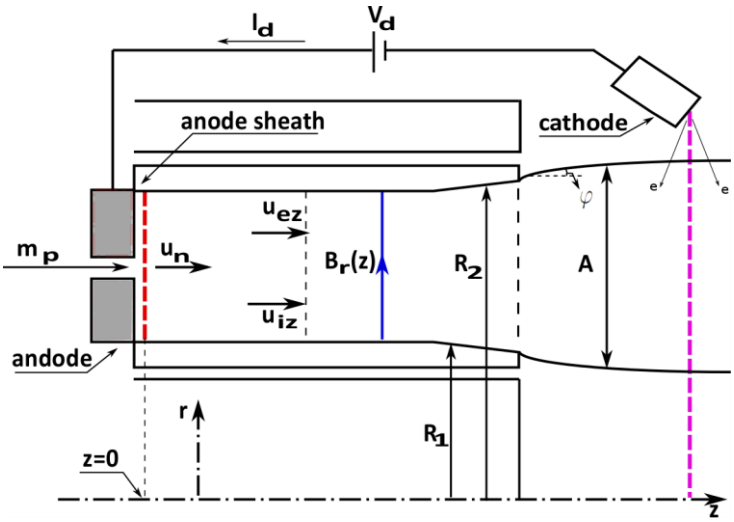

Figure 1. Hall thruster geometrical scheme

In order to reduce the model complexity, all the plasma proprieties within the channel and the plume are considered in stationary conditions. Moreover, we assume that the plasma and neutral flows can be described in terms of radially averaged fields, which depend on the axial coordinate z only.
We consider a three-fluid description of the plasma, where the properties of electrons (e), ions (i), and neutrals (n) are indicated by the corresponding letters as subscript. Since in a Hall thruster the Debye length is much smaller than the characteristic length scale, we assume that the plasma is quasi-neutral, i.e. the electron and ion particle densities are in local balance, $n_i = n_e \stackrel{\text{def}}{=} n$. The regions near the walls, where the quasi-neutrality is violated, will be the object of a specific analysis in Section 2.2.
The potential drop between the anode and the cathode is assumed equal to the discharge voltage V_d, whereas the current provided by the cathode is the discharge current I_d. The neutrals are injected from the anode with a mass flow rate $\dot{m}_p$.
The magnetic field is assumed purely radial and a function of the axial coordinate, $\vec{B} = B_r(z)\hat{e}_r$. The magnetic field induced by the plasma currents is neglected. The assumption allow us to write the electric field as $\vec{E} = E_z\hat{e}_z = -\nabla\phi$.
The equations governing the plasma and neutral flows can be written as

$$\frac{d}{dz}(nu_{iz}A) = n(\nu_I - \nu_w)A\,, \tag{1}$$

$$\frac{d}{dz}(nu_{ez}A) = n(\nu_I - \nu_w)A\,, \tag{2}$$

$$\frac{d}{dz}(n_n u_{nz}A) = -n(\nu_I - \nu_w)A\,, \tag{3}$$

$$\frac{d}{dz}(m_i n u_{iz}^2 A) = -en\frac{d\phi}{dz}A + m_i\, n(\nu_I u_{nz} - \nu_w u_{iz})A\,, \tag{4}$$

$$0 = en\frac{d\phi}{dz} - \frac{d}{dz}(nk_B T_e) - m_e\, n\frac{\omega_e^2}{\nu_e}u_{ez}\,, \tag{5}$$

$$\frac{d}{dz}\left(\frac{5}{2}nk_B T_e u_{ez}A\right) = enu_{ez}\frac{d\phi}{dz}A - n(\nu_I \alpha_I \Sigma_I + \nu_{we} T_e)A\,, \tag{6}$$

where u_{iz}, u_{ez}, u_{nz} indicate the axial component of the ion, electron, and neutral velocity respectively, ϕ is the plasma potential, T_e is the electron temperature, n is the plasma density, n_n is the neutral density, k_B is the Boltzmann constant, m_i, m_e and e are the ion mass, the electron mass and the electron charge respectively, and $\omega_e = eB/m_e$ is the electron cyclotron frequency.

Eqs. (1), (2), and (3) represent the conservation of ion, electron, and neutral particles respectively. The ionization frequency ν_I can be expressed as

$$\nu_I = n_n R_I(T_e)\,, \tag{7}$$

where $R_I(T_e)$ is the effective ionization rate (in the Appendix we report the expressions of $R_I(T_e)$ used), whereas particle recombination at the channel walls is described by the equivalent frequency ν_w.

Eq. (4) represents the conservation of the ion momentum. Since the Larmour radius of the ions is much larger than the typical dimensions of the thruster, the ions are considered as non-magnetized. Furthermore, in Eq. (4) we neglected the effect of the ion pressure, considering the ions as a cold specie. This assumption, which is justified by the fact that the ion temperature is significantly lower than the electron temperature [6], allows us to discard the ion energy equation from the model.

Eqs. (5) and (6) represent the conservation of the electron momentum and energy respectively. In both these equations, due to the very low mass of the electrons, we neglected the inertial terms. Moreover, we neglected heat conduction and we assumed a Maxwellian distribution function for the electrons. Consequently, the electron pressure P_e was written as

$$P_e = nk_B T_e\,. \tag{8}$$

The value α_I that appears in Eq. (6) takes into account the effective energy loss per actual ionization ($\alpha_I \sim 2-3$)[6], whereas Σ_I is the ionization energy of the propellant gas ($\Sigma_I = 12.1\ eV$ for xenon).

In the derivation of Eq. (5), we exploited the azimuthal electron momentum equation, $u_{e\theta} = -\omega_e u_{ez}/\nu_e$, where $u_{e\theta}$ indicates the azimuthal component of the electron velocity, together with the assumption of a Hall parameter (β_e) significantly greater than one, $\beta_e = \omega_e/\nu_e \gg 1$.

The effective electron collision frequency, ν_e, is the sum of the electron-neutral collision frequency (ν_{en}), the electron-ion collision frequency (ν_{ei}), the Bohm collision frequency (ν_B) and the near-wall collision frequency (ν_{ew})

$$\nu_e = \nu_{en} + \nu_{ei} + \nu_B + \nu_{ew}\,. \tag{9}$$

Since electron-ion collisions typically give a negligible contribution to ν_e [6], we can neglect them in the following. On the other hand, the electron-ion collision frequency, ν_{en}, can be written as

$$\nu_{en} = n_n \sigma_{en}\sqrt{\frac{8k_B T_e}{\pi m_e}}\,, \tag{10}$$

where σ_{en} is the electron-neutral collision cross section. The latter is a function of the electron temperature but, in the electron temperature range of interest for Hall effect thrusters (few tens of eV), σ_{en} can be considered constant [6]. In particular $\sigma_{en} \cong 27 \cdot 10^{20}\ m^2$ for Xe, approximating experimental data of Ref. [9].

The Bohm collision frequency takes into account the contribution to electron transport due to plasma oscillations and can be written as

$$\nu_B = \alpha_B \omega_e\,, \tag{11}$$

where α_B is the Bohm coefficient. In general, the latter is a function of both the axial coordinate and the operating condition of the thruster. Nevertheless, we used a constant value of α_B for the whole domain (as previously done by other authors [1], [6]-[8]). However, as explained in Section 3.2, a functional dependence of the Bohm parameter on the thruster operating condition is assumed, in particular relating α_B with the discharge voltage V_d.
The effect of plasma-wall interactions on the electron mobility are introduced by the equivalent collision frequency [1], [8]

$$\nu_{ew} = \frac{\gamma}{1-\gamma}\nu_w \,, \tag{12}$$

where γ is the secondary emission yield.
Furthermore, energy losses due to ionization are introduced via a volumetric energy sink, whereas the energy loss at the channel walls is described by the equivalent frequency ν_{we}.
For what concerns the neutral dynamics, we assume a constant velocity of the neutrals within the channel and the plume. Hence, no neutral momentum and energy equation is included in the formulation of the model. The latter assumption is found to be a good approximation regarding the neutral dynamics in Hall thrusters [10]. In particular, the value of the neutral velocity can be written as [10]

$$u_{nz} = \sqrt{\frac{8\alpha k_B T_a}{\pi m_i}} \,, \tag{13}$$

where T_a is the anode temperature and α is the neutral temperature accommodation factor, ($\alpha = 0.25$). The anode temperature is related to the power deposited at the anode, and the latter is proportional to the discharge current. The relation between T_a and I_d clearly depends on the specific thruster model under consideration, in particular, in the case of the HT5k we approximated experimental data regarding the anode temperature at various operating conditions obtaining the dependence $T_a = T_a(I_d)$.

2.2 Wall Interaction Terms

The adoption of a radially averaged description of the plasma flow reduces the model complexity. However, the radial boundaries of the domain have a strong influence on the plasma behaviour and the effects of these boundaries need to be included in the model. As illustrated in the previous section, particle recombination and energy losses at the walls can be effectively modeled by means of volumetric source terms. In order to find analytical expressions for the representative frequencies, ν_w and ν_{we}, we have to investigate the radial behaviour of the plasma inside the channel.
Under the assumption of a radial magnetic field, the plasma radial behaviour corresponds to the behaviour along a magnetic field line. In the following, we also assume that the channel presents small azimuthal curvature and, thus, it can be considered quasi-planar and symmetric with respect to the channel centerline.
Under these conditions, we performed an asymptotic analysis of the plasma behaviour in the radial direction. Following the classical sheath description, we identified a non-collisional sheath region (a few Debye lengths thick, next to the wall), where quasi-neutrality is violated, and a collisional, quasi-neutral pre-sheath (from the channel centerline to the plasma edge of the sheath). For the ceramic material and propellant under analysis, the sheath model of Ref. [5], and [11] yields all the relevant plasma properties at the wall as a function of the local "bulk" properties. In particular, given the values of plasma density and electron temperature at the sheath entrance, we can deduce the radial velocity of the incoming ions (u_{ir0}), the total potential drop through the sheath (ϕ_{sh}), the ion flux to the walls (Γ_{iw}), and the power deposited to the walls (P_w). However, since the 1D axial model is expressed in terms of averaged fields, we need to assess the ratio between the plasma density at the plasma edge of the sheath, n_0, and the average density on a channel cross section, n.
Let us consider the conservation equations of ion momentum in the pre-sheath

$$m_i \hat{n} u_{ir} \frac{\partial u_{ir}}{\partial r} = -e\hat{n}\frac{\partial \phi}{\partial r} - m_i \hat{n} \nu_I u_{ir} \,, \tag{14}$$

where we introduced the notation $\hat{n}$ to indicate the local plasma density, which depends on the radial coordinate.
By neglecting the ionization contribution and integrating Eq. (14) from the channel centerline (where $u_{ir} = 0$) to the sheath edge (where $\phi = 0$ and $u_{ir} \approx u_B$, the classical Bohm velocity), we obtain, as a first approximation, the plasma potential drop from the centerline to the sheath

$$\phi_M = k_B T_e / 2e \,, \tag{15}$$

which also expresses the ion energy conservation. Then, calling n_M the plasma density at the channel centerline, if we consider the Boltzmann relationship for plasmas with maxwellian electron distribution functions

$$n_M = n_0 \exp\left(\frac{e\phi_M}{k_B T_e}\right), \tag{16}$$

and we assume a linear radial profile for the plasma density $n = (n_0 + n_M)/2$, we obtain

$$\frac{n_0}{n} = \frac{2}{1 + \exp(1/2)}. \tag{17}$$

Due to the strong simplifications used in the derivation of Eq. (17), we introduce a factor (f) to express the uncertainty in the radial plasma behavior. The parameter needs to be calibrated on the specific thruster and, since this factor mainly depends on the effect of the ionization in the pre-sheath, we assumed a linear dependence of f on the neutral density at the anode.

By using Eq. (17), the equivalent volumetric source frequencies for both the particle ν_w and energy ν_{we} exchange through the lateral walls can be obtained. For what concerns the particle exchange, we impose that

$$\Gamma_{iw} = n \nu_w A dz \,, \tag{18}$$

and that the ion flux to the walls, Γ_{iw}, can be written using the expression of Ref. [5]. After substitution, the expression for the particle-wall interaction frequency results

$$\nu_w = \frac{f}{1 + \exp(1/2)} (1 - \gamma) \left(\frac{8 k_B T_e}{\pi m_e}\right)^{\frac{1}{2}} \exp\left(\frac{e\phi_{sh}}{k T_e}\right) \frac{1}{R_2 - R_1}. \tag{19}$$

Next, in order to find the expression for the energy loss through the lateral walls, we consider the balance between the power flux to the walls, P_w (for a detailed description see Ref. [5]), and the equivalent volumetric energy loss

$$P_w = n k_B T_e \nu_{we} A dz \,. \tag{20}$$

Hence, the expression for the energy-wall interaction frequency can be written as

$$\nu_{we} = \frac{f}{1 + \exp(1/2)} \left(\frac{8 k_B T_e}{\pi m_e}\right)^{\frac{1}{2}} \exp\left(\frac{e\phi_{sh}}{k T_e}\right) \frac{2}{R_2 - R_1}. \tag{21}$$

2.3 Plume Divergence Law

A law for the expansion of the plasma, dA/dz, is needed to complete the equations in the near-plume region (from the channel exit to the cathode).

For a cylindrical plasma flow, with $\varphi(z)$ the local divergence angle, the area variation in the plume $(z > L_{ch})$ verifies

$$\frac{d}{dz} \ln(A) = \frac{2}{R_2 - R_1} \tan(\varphi) \,. \tag{22}$$

We assume that, in the near-plume, the gas expands radially with the local value of the Bohm velocity $\left(u_B = \sqrt{k_B T_e / m_i}\right)$, describing a "diffusive process", which implies that we take

$$\tan(\varphi) = \frac{u_B}{u_{iz}} = \frac{\sqrt{k_B T_e / m_i}}{u_{iz}} \,. \tag{23}$$

For what concerns the far-plume region ($z > L_{cat}$), we assume that the behaviour of the current-free plasma there has a negligible influence on the thruster operation.

2.4 Boundary Conditions

In order to close the numerical problem and to integrate the system of Eqs. (1)-(6), we need to define six boundary conditions that correctly represent the given problem. Although the choice of such conditions is not unique, observations about the physical nature of the problem led to the identification of the following set of boundary conditions.
First, we assume to know the electron temperature at the cathode, which is experimentally verified to be of the order of the electron emission temperature [6],

$$T_e(L_{cat}) = T_{e(cat)} \,. \tag{24}$$

Then, due to the fact that the definition of the electric potential is unique up to an additive constant, we set the reference value of ϕ equal to zero at the cathode,

$$\phi(L_{cat}) = 0 \,. \tag{25}$$

The potential drop between the anode and the cathode, V_d, is known. Notice that the plasma is considered quasi-neutral, therefore, the anode sheath is excluded from the computational domain. Hence, we have $\phi(0) - \phi(L_{cat}) = \phi(0) = V_d + \phi_{Ash}$, where ϕ_{Ash} represents the potential drop in the anode sheath. ϕ_{Ash} usually is much smaller compared to V_d, consequently, we decide to neglect it. Hence, the condition on the potential imposed at $z = 0$ is

$$\phi(0) = V_d \,. \tag{26}$$

Furthermore, we assume a plasma density at $z = 0$ two orders of magnitude lower than $n_n(0)$,

$$n(0) = \frac{n_n(0)}{100} \,. \tag{27}$$

Although somewhat arbitrary, notice that due to the large ionization efficiency of Hall thrusters, the effective value of the plasma density at the anode is expected to only marginally affect the solution.
Moreover, we impose the value of the ion velocity in $z = 0$,

$$u_{iz}(0) = u_{iz0} \,. \tag{28}$$

For typical Hall thruster operation conditions, the sheath at the anode surface is electron repelling [12]. Therefore, the most physical condition for u_{iz0}, is the imposition of the Bohm velocity directed towards the anode,

$$u_{iz}(0) = u_{iz0} = -u_B(0) = -\sqrt{\frac{k_B T_e(0)}{m_i}} \,. \tag{29}$$

However, the ions are accelerated through the potential drop between anode and cathode, thus, a negative u_{iz0} implies the presence of a point within the channel where the ion velocity becomes equal to zero. The presence of this particular point involves numerical problems that are analyzed in Section 2.5.
For what concerns the neutral density, notice that the anode propellant mass flow rate ($\dot{m}_p$) and the anode neutral velocity (u_{nz}) are both known. Therefore, the application of the mass continuity equation at $z = 0$ yields

$$n_n(0) = \frac{\dot{m}_p}{m_i A(0) \left(u_{nz} + \frac{n_n(0)}{n(0)} u_{iz}(0) \right)} \,. \tag{30}$$

Observe that, since these boundary conditions are applied at different axial locations of the computational domain, an iteration procedure is needed to integrate Eqs. (1)-(6).

2.5 Sensitivity Analysis

With the aim of integrating Eqs. (1)-(6) it is convenient to use dimensionless variables. In order to obtain a non-dimensional form of Eqs. (1)-(6), we identified a set of reference quantities:

$$T_{ref} = \frac{\Sigma_I}{k_B}, \qquad \omega_{ref} = \frac{eB_m}{m_e}, \qquad L_{ref} = L_{ch}, \qquad \sigma_{ref} = \sigma_{I0}\sqrt{\frac{m_i}{m_e}},$$

where B_m indicates the peak value of the magnetic field induction. Moreover, we used the quantities defined above to define the reference values

$$n_{ref} = \frac{1}{L_{ref}\sigma_{ref}}, \qquad v_{ref} = \frac{u_{ref}}{L_{ref}}, \qquad u_{ref} = \sqrt{\frac{k_B T_{ref}}{m_i}}, \qquad \phi_{ref} = \frac{k_B T_{ref}}{e}.$$

The dimensionless form of Eqs. (1)-(6) is straightforward to obtain and is not presented in this document. However, dimensionless magnitudes will be represented by a tilde over the respective dimensional ones.
As discussed in Ref. [6], the set of Eqs. (1)-(6), due to the effect of the electron pressure gradient, presents a singular point for $M^2 = 1$, where $M = \tilde{u}_{iz}/\sqrt{5\tilde{T}_e/3}$ is the Mach number. The sonic transition of the ion flow implies numerical complications in the integration of the final set of equations. In particular, to solve the problems related with the ion sonic transition, Ahedo et al. [6] developed an ad-hoc procedure based on the direct integration of the equations from the sonic point inwards to the anode, and outwards to the cathode.
In order to simplify the numerical procedure, we analysed the effects of the electron pressure on the thruster performance. We simulated a typical operating condition of an SPT-100, neglecting the plume expansion, and we compared the plasma behavior with and without the pressure term. Figure 2 shows the results of the analysis.

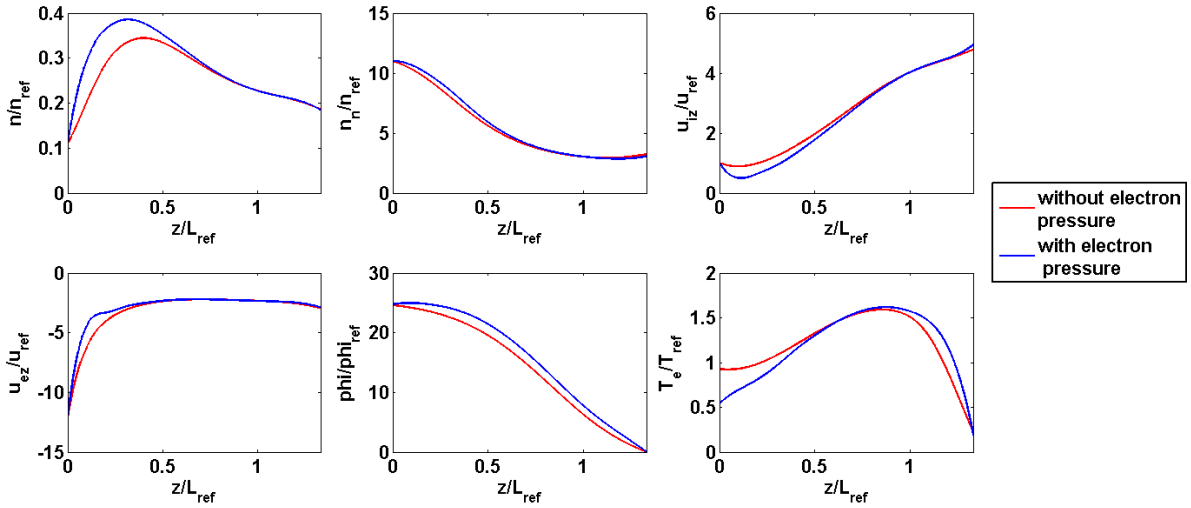

Figure 2. Effect of the electron pressure on the solution.

The profiles present only small differences, confined in a limited region near the anode. The values of the various plasma proprieties converge at a certain distance from the anode and the peaks do not present significant variations. Therefore, we decided to neglect the electron pressure in Eq. (5), allowing for a significant reduction of the model complexity. By neglecting the electron pressure, we inevitably introduce errors in the evaluation of the plasma proprieties. In particular, we expect to overestimate the electric field in the near anode region, and to underestimate it near the channel exit. This does not jeopardize the prediction of the thruster performance; however, it influences the erosion calculation, as explained in Section 3.5.
A similar analysis was then performed to assess the influence of the ion velocity at the anode. Indeed, by neglecting the pressure contribution in the ion momentum equation, numerical complications occur when the ion velocity becomes equal to zero, $\tilde{u}_{iz} = 0$. Such complications can be easily avoided imposing a positive value for the ion

velocity at $z = 0$. The performed analysis showed that, except for the region close to the anode, changes of the boundary value of u_{iz} in the range $-u_B$ and $+500\, m/s$ produce negligible effects on the plasma fields. In particular, since the ions are generated, through ionization, at the same velocity of the neutrals, we decided to use $\tilde{u}_{iz0} = \tilde{u}_{nz}$ as boundary condition for the ion velocity.

2.6 Erosion Model

Once the model is integrated and all the plasma properties profiles are known in the channel and near plume, the data can be used as an input to compute the erosion rate of the ceramic walls.
The calculation of the erosion rate is performed using the semi-empirical dependence of the sputtering yield presented in Ref. [5], and [13], where experimental data [14] are used to extrapolate a dependence of the sputtering yield (Y in mm^3/C) on both the ion kinetic energy (E_i in eV) and the impact angle (δ in degrees). In particular, for the case of singly ionized xenon ions impacting on $BNSiO_2$ ceramic walls, the semi-empirical fit can be expressed as

$$Y = (0.0099 + 6.04 \cdot 10^{-6}\delta^2 - 4.75 \cdot 10^{-8}\delta^3)\sqrt{E_i}\left(1 - \sqrt{\frac{E_{th}}{E_i}}\right)^{2.5}, \tag{31}$$

where E_{th} is an empirical constant that represents the threshold energy, in eV, under which no sensible erosion is recognized.
With the ion current per unit surface to the wall (J_{iw}) given by the model solution, the erosion rate in the direction orthogonal to the wall can be simply computed as

$$\varepsilon = Y J_{iw}\,. \tag{32}$$

Then, for short time intervals Δt, we assume that the change of the channel area has a negligible impact on the plasma properties and we evaluate the actual erosion as the product between the erosion rate and Δt. The channel geometry is then modified according to the computed erosion and the model is integrated again. The iterative process is stopped when the desired operation time is achieved.

3. Model Results: HT5k

This section presents the solutions predicted by the model for the plasma behaviour inside the HT5k, Sitael's 5kW class thruster, and reports the comparison between the computed performance and the experimental measurements.
The HT5k (see Fig. 3) is a Hall Effect thruster designed to work in the power range 3-7 kW. The thruster can operate in a wide range of operating points, among which two distinct nominal modes for a given power level can be identified: the High Thrust mode, suitable for orbit insertion, orbit raising or repositioning, and the High Specific Impulse mode, typically used for station-keeping applications.
The discharge chamber of the thruster is an annular U-shaped channel of ceramic material composed by boron nitride (BN) and silicon dioxide (SiO2). The HT5k is usually equipped with a HC20 high-current hollow cathode, developed by Sitael in the past few years.

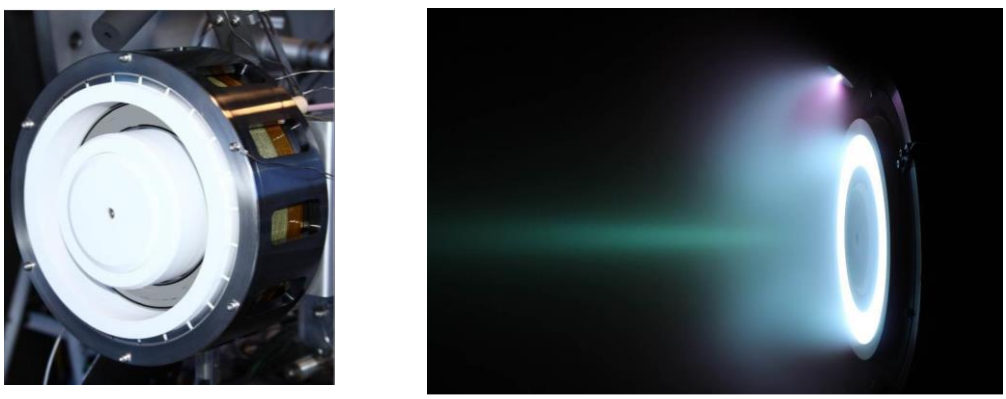

Figure 3: The HT5k thruster mounted on the thrust balance (left) and during operation (right).

All elements of the thruster magnetic circuit are made of soft magnetic alloy and, when magnetized by coils, allow producing an almost radial magnetic field at the exit plane of the thruster accelerating channel, with a nominal peak value of 0.019 T.
The nominal operating parameters, considered in this study, for the HT5k, refer to the high thrust mode of the thruster, with a nominal operating power of 5000 W, a discharge voltage of 300 V and a xenon mass flow rate of 16.5 mg/s.
An accurate experimental characterization of thruster performance was carried out in Sitael's testing facilities. Further details of the experimental campaign can be found in Ref. [15].
In the following, the model capability to accurately predict the performance of real thrusters is thoroughly verified on the HT5k, also far from the nominal operating point. Moreover, an analysis of the computed plasma and performance parameters in the high thrust nominal condition of the thruster operating with xenon is reported. Finally, the erosion calculation and the comparison with experimental data for a specific operating condition is presented.

3.2 Nominal Operating Condition

In order to predict the HT5k performance, the two free parameters of the model f, α_B, and the anode temperature T_a, must be calibrated with experimental data.
For the anode temperature we assumed a linear dependence over the discharge current, approximating it from experimental measurements.
Then, in order to calibrate f and α_B,, we analysed a wide range of operating conditions and performed a linear approximation to match the experimental performance. Based on the data collected, we approximated f as linearly dependent on the anode neutral density $n_n(0)$, and $1/\alpha_B$ as linearly dependent on V_d.
In particular, f ranges from 0.75 to 1.19. This implies that the simplified pre-sheath model described in Section 2.2 is reasonably accurate.
Once the relation between f, α_B, T_a, and the thruster operating condition were defined, we used the 1D model to compute the plasma proprieties within the channel and the near plume. The results for the high thrust nominal operating point of the HT5k, with xenon as propellant, are shown in Fig. 4.

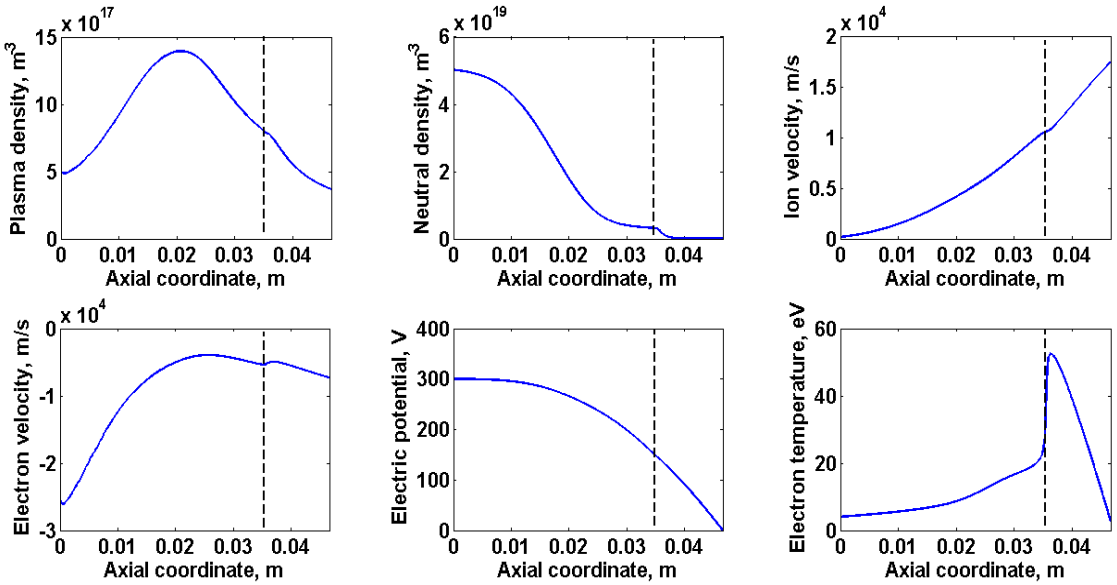

Figure 4. HT5k plasma proprieties. High thrust nominal operating point: $V_d = 300\ V$, $\dot{m}_P = 16.5\ mg/s$, $I_d = 16.7\ A$, $P = 5000\ W$. The dashed lines indicate the axial location of the channel exit.

The profiles presented in Fig. 4 are in accordance with the results obtained by other authors [16], [17], and have some features that deserve to be outlined. The derivative of the plasma proprieties present a discontinuity in correspondence of the channel exit. This is due to the area change outside of the thruster, and because in the near plume the wall effects rapidly vanish.
The disappearance of the wall effects outside of the thruster is also the reason behind the external electron temperature peak. Indeed, the channel walls act as an energy sink and do not allow a strong increment of the electron

temperature inside the thruster [18]. Whereas, outside of the channel the plasma is not bounded and the effect of the walls vanishes. Thus, in the near plume the electron temperature is able to increase and rise up to values of about 50 eV.

3.4 Thruster Performance

Based on the prediction of the plasma properties at the cathode section, we computed the thruster performance for a wide range of operating conditions. Given the one-dimensional plasma properties, the thrust was computed as $T = (m_i n_i u_i{}^2 A)_{z=Lcat}$, and the anodic specific impulse as $I_{spA} = T/(g_0 \dot{m}_P)$, where g_0 is the standard acceleration due to gravity at sea level. Lastly, the anodic thrust efficiency was computed as $\eta_A = T^2/(2\dot{m}_p I_d V_d)$.
In Fig. 5 the comparison between performance predictions (solid lines) and experimental data (diamonds) is presented.

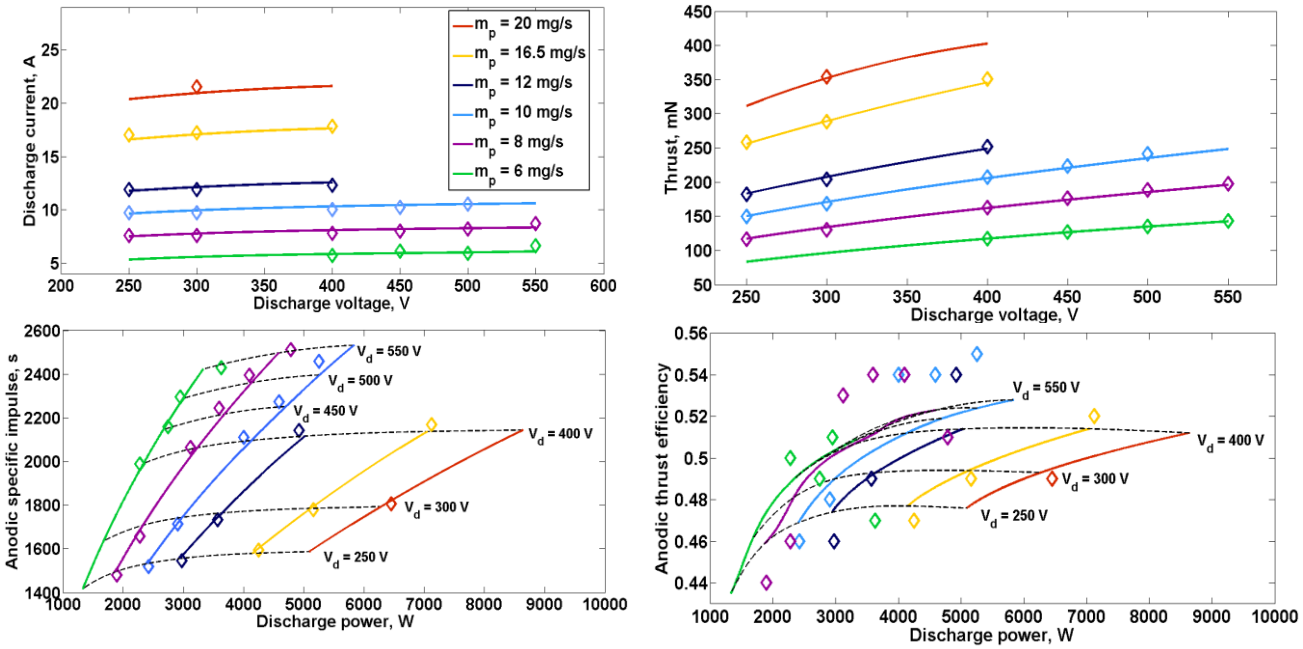

Figure 5. Comparison between predicted performance parameters and experimental data of the HT5k.

As it is evident from Fig. 5, extremely small differences between the prediction and the experimental data are recorded for the directly measured quantities, i.e. the discharge current and the thrust, with errors below 5% also far from the nominal operating point. Slightly higher differences are found for the performance parameters not directly measured, but computed a posteriori, in particular for the anodic thrust efficiency. This trend is to be attributed to the accumulation of the experimental errors, and do not compromise the validity of the simulations.

3.5 Channel Erosion

Erosion measurements were performed on a specific operating condition of the thruster, with a discharge power of 4370W and a discharge voltage of 300V.
We simulated the plasma behaviour inside the thruster and computed the erosion rate of the channel walls for this condition. Then, we compared the outer wall eroded experimental profile after 33 h of operation with the numerically predicted one. The results are presented in Fig.6.
The channel erosion is extremely sensitive to local plasma parameters, in particular near the channel exit, where the gradients of plasma properties are stronger. Neglecting the effect of the electron pressure has practically no influence on the prediction of the performance parameters, but implies a lower plasma potential at the channel exit. Hence, the model predicts a higher kinetic energy of the ions inside the channel. Furthermore, we assumed that the plasma properties are constant during each computational time step. In the end, an over-prediction of the erosion rate is expected.

Although no direct experimental estimate for the value of E_{th} could be found in literature, Goebel et al. in Ref. [5] suggest a value of $E_{th} = 58.6\ eV$ to fit the higher energy experimental points. Using this value, the model over-predicts the erosion of the channel walls (dashed line in Fig. 6). Different values of the energy threshold are reported, for example, in Ref. [12], $E_{th} \cong 60\ eV$, and in Ref. [19], E_{th} between 30 and 70 eV.
The erosion is strongly influenced by the value of E_{th}. Using a slightly higher value of the threshold energy, $E_{th} = 84\ eV$ (solid line in Fig. 6), the erosion calculated is in substantial agreement with the experimental measurements.

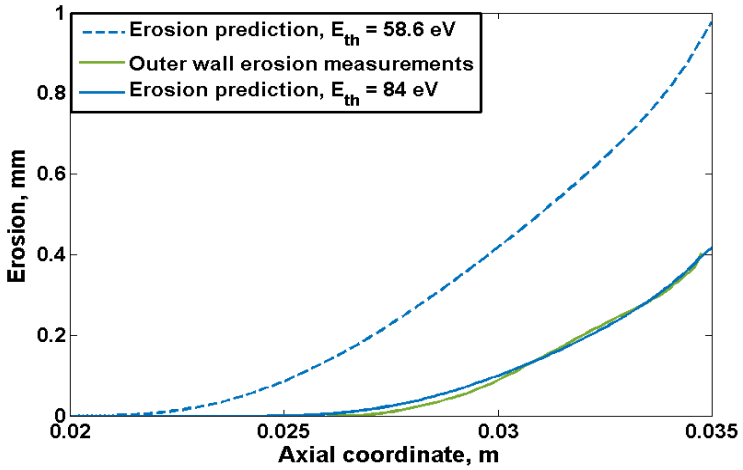

Figure 6. Erosion prediction for the HT5k with different energy thresholds against erosion measurements on the outer wall after 33 h of firing

The difference between the fitting value of E_{th} and the values proposed by other authors can be ascribed to both the uncertainties on the physical value of E_{th} and the approximations introduced in the model.

4. Model Results: SPT-100

In order to further assess the reliability of the model, the operations of the SPT-100 thruster were investigated. In order to study the thruster behaviour, we calibrated the two free parameters of the model (f, α_B) using experimental results, described for example in Refs. [20] and [21]. The calibration showed a weak dependence of the parameter f on the operating condition, thus, we assumed a constant $f = 1.18$.
A comparison between the model predictions and the thruster performance was then performed.

4.2 Thruster Behaviour

The baseline operating point of the SPT-100 is characterized by a discharge voltage of 300 V and a discharge power of 1350 W. Several operating conditions of the thruster were simulated. The general trends of the plasma properties inside the channel, presented in Fig. 7 for the nominal operating point, are similar to the ones previously described for the HT5k, although the electron temperature for the case of the SPT-100 is lower, with a peak value of ~30 eV. For the case of the SPT-100, the performance predictions are in good agreement with the measured performance, also far from the nominal operating point, with errors always below the 5%. The highest discrepancies are found again on the non-directly measured quantities, such as the anodic specific impulse and the thrust efficiency.

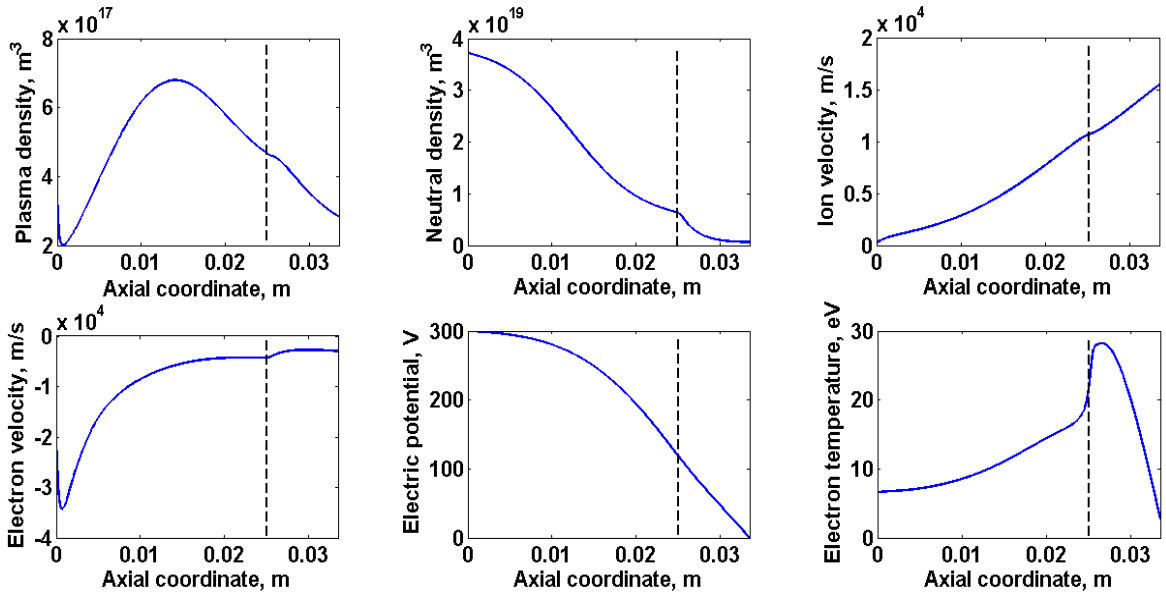

Figure 7. SPT-100 plasma proprieties. Nominal operating point: $V_d = 300\ V$, $P = 1350\ W$. The dashed lines indicate the axial location of the channel exit.

4.3 Channel Erosion

By using the same value of the threshold energy defined in Section 3.5, we calculated the erosion of the channel walls of the SPT-100 when operated at the baseline condition. We assessed the channel erosion up to 800h of thruster operations, with a time-step $\Delta t = 30h$. Then, we compared the results with the erosion measurements reported by Absalamov et al. in Ref. [22].

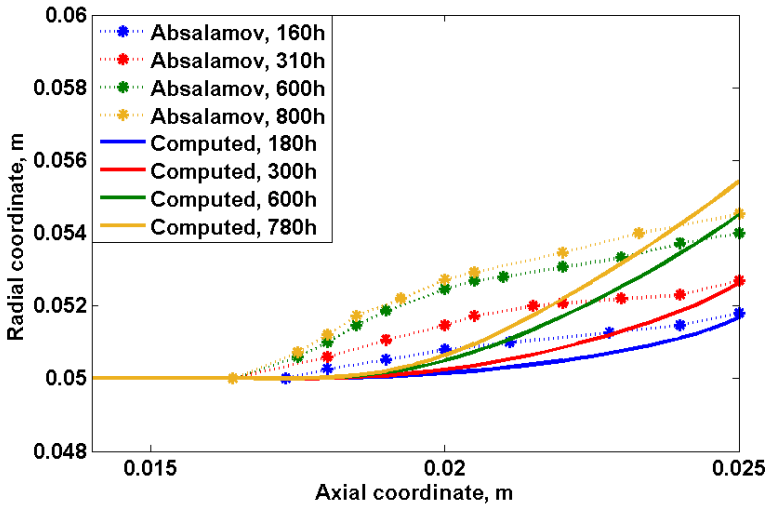

Figure 8. Erosion prediction for the SPT-100 against erosion measurements on the outer wall at different times

As shown in Fig. 8, the model overestimates the erosion of the ceramic at the channel exit and underestimates it inside the channel. A first cause of the observed discrepancy is probably related with the assumption of a purely radial magnetic field. Indeed, near the walls, the change of inclination between the magnetic field and the ceramic surface is expected to have a significant influence on the flux of energetic particles. Moreover, neglecting the

electron pressure also affects the erosion predictions. Even if the electron pressure has a minor influence on the thruster performance, the effect of the electron pressure is to flat down the temperature profile and to move the accelerating layer out of the channel, thus reducing the energy of ions that flow to the walls. A slight discrepancy in the erosion rate between the model results and the real thruster conditions generates, for long erosion times, the differences observed in Fig. 8. Further investigations are thus needed to assess the specific role of the highlighted effects.

5. Conclusions

A one-dimensional model of Hall thrusters was developed and validated on the HT5k and the SPT-100. The model includes the effects of plasma-wall interactions, propellant ionization, neutral dynamics and plume expansion. A sensitivity analysis of the effects, on the plasma dynamic, of the electron pressure and of the anode boundary condition for the ion velocity was performed. The results showed a relevant effect only in a limited region near the anode. Therefore, we decided to discard the electron pressure from the model and to impose a positive ion velocity at the anode, equal to the neutral one, allowing for a significant simplification of the numerical integration procedure. We investigated the neutral dynamic inside the channel, and the neutral velocity was related to the discharge current. The model contains two free parameters: f and α_B. The former takes into account the uncertainties present in the description of the plasma-wall interaction, while the latter allows for the inclusion of the effects of plasma oscillations on electron transport. The role of f and α_B was investigated over a wide range of operating conditions. In particular, we linked f and α_B, through a linear approximation of the data collected, to the value of the neutral density at the anode and with the thruster discharge voltage, respectively.
The model was used to predict the performance of the thrusters for different operating conditions. Computed and experimental performance are in agreement within an error lower than 5%. The model is able to catch the main features of the plasma proprieties within the channel and in the near plume. Then, a specific operating condition was considered and the erosion of the channel walls was computed. By fitting the threshold energy of the ceramic sputtering yield function with experimental data, the model is able to reasonably predict the channel erosion rates.

Appendix

The ionization rate can be expressed as $R_I(T_e) = \sigma_I(T_e)\sqrt{8k_B T_e/(\pi m_e)}$
The expression for the ionization cross section $\sigma_I(T_e)$ described in Ref. [6] was used

$$\sigma_I(T_e) = \sigma_{I0}\left(1 + \frac{k_B T_e \Sigma_I}{(k_B T_e + \Sigma_I)^2}\right)\exp\left(-\frac{\Sigma_I}{k_B T_e}\right), \tag{A1}$$

where σ_{I0} is a semi-empirical constant that we obtained, for xenon, integrating the experimental data in Ref. [9]: $\sigma_{I0\,Xe} = 5 \cdot 10^{-20}\, m^2$.

Acknowledgements

This work was supported by Sitael S.p.A.

References

[1] Fife, J. M. 1998. Hybrid-PIC Modeling and Electrostatic Probe Survey of Hall Thrusters. Ph.D. Dissertation, Aeronautics and Astronautics, Massachusetts Institute of Technology
[2] Mikellides, I. G., Katz, I., Hofer, R. R., and Goebel, D. M. 2010. Magnetic Shielding of the Acceleration Channel Walls in a Long-Life Hall Thruster. *46th AIAA/ASME/SAE/ASEE Joint Propulsion Conference & Exhibit*, AIAA 2010-6942.
[3] Mikellides, I. G., Katz, I., Hofer, R. R. 2011. Design of a Laboratory Hall Thruster with Magnetically Shielded Channel Walls, Phase I: Numerical Simulations. *44th AIAA/ASME/SAE/ASEE Joint Propulsion Conference & Exhibit*, AIAA 2011-5809.

[4] Mikellides, I. G., Katz, I., Hofer, R. R., and Goebel, D. M. 2014. Magnetic shielding of a laboratory Hall thruster. I. Theory and validation. *Journal of Applied Physics*, Vol. 115, pp. 043303.
[5] Goebel, D. M., and Katz, I. 2008. *Fundamentals of Electric Propulsion: Ion and Hall Thrusters*. Wiley, Hoboken N.J.
[6] Ahedo, E., Martinez-Cerezo, P., and Martinez-Sanchez, M. 2001. One-dimensional model of the plasma flow in a Hall thruster. *Physics of Plasmas*, Vol. 8, No. 6, pp. 3058-3067.
[7] Ahedo, E., Gallardo, J., and Martinez-Sanchez, M. 2002. Model of the plasma discharge in a hall thruster with heat conduction. *Physics of Plasmas*, Vol. 9, No. 9, pp. 4061-4070.
[8] Ahedo, E., Gallardo, J., and Martinez-Sanchez, M. 2003. Effect of the radial plasma-wall interaction on the Hall thruster discharge. *Physics of Plasmas*, Vol. 10, No. 8, pp. 3397-3409.
[9] Linnel, J. A. 2007. An Evaluation of Krypton Propellant in Hall Thrusters. Ph.D. dissertation, University of Michigan, Ann Arbor, MI.
[10] Reid, B., "The Influence of Neutral Flow Rate in the Operation of Hall Thrusters," Ph.D. dissertation, University of Michigan, Ann Arbor, MI, 2009.
[11] Hobbs, G. D., and Wesson, J. A. 1967. Heat Flow Through a Langmuir Sheath in the Presence of Electron Emission. *Plasma Physics*, Vol. 9, pp. 85–87.
[12] Ahedo, E., Escobar, D. 2008. Two-region model for positive and negative plasma sheaths and its application to Hall thruster metallic anodes. *Physics of Plasmas*, Vol. 15, pp. 033504.
[13] Gamero-Castaño, M., and Katz. I. 2005. Estimation of Hall Thruster Erosion Using HPHall. In *Proceedings of the 28th International Electric Propulsion Conference*, IEPC Paper 2005-303.
[14] Garnier, Y., Viel, V., Roussel, J.-F., Pagnon, D., Magne, I., and Touezau, M. 1999. Investigation of xenon ion sputtering of one ceramic material used in SPT discharge chamber. In *Proceedings of the 34th International Electric Propulsion Conference*, IEPC 1999-83.
[15] Ducci, C., Arkhipov, A., and Andrenucci, M. 2015. Development and performance characterization of a 5 kW class Hall-Effect thruster. In *Proceedings of the 26th International Electric Propulsion Conference*, IEPC 2015-215. (to be presented)
[16] Anton, A., Escobar, D., and Ahedo E. 2006. Contour algorithms for a Hall thruster hybrid code. *42nd AIAA/ASME/SAE/ASEE Joint Propulsion Conference & Exhibit*, AIAA 2006-4834.
[17] Hofer, R. R., Mikellides, I. G., Katz, I., and Goebel, D. M. 2007. Wall Sheath and Electron Mobility Modeling in Hybrid-PIC Hall Thruster Simulations. *43rd AIAA/ASME/SAE/ASEE Joint Propulsion Conference & Exhibit*, AIAA 2007-4834.
[18] Choueiri, E. Y. 2001. Fundamental Difference Between Two Variants of Hall Thrusters: SPT and TAL. *Physics of Plasmas*, Vol. 8, No. 11, pp. 5025–5033.
[19] Garrigues, L., Hagelaar, G.J.M., Bareilles, J., Boniface, C., and Boeuf, J. P. 2003. Model study of the influence of the magnetic field configuration on the performance and lifetime of a Hall thruster. *Physics of Plasmas*, Vol. 10, No. 12, pp. 4886-4892.
[20] Sankovic, J.M., Hamley, J.A., and Haag, T.W. 1994. Performance Evaluation of the Russian SPT-100 Thruster at NASA LeRC. In *Proceedings of the 23rd International Electric Propulsion Conference*, IEPC 1993-094.
[21] Manzella, D., Jacobson, D., and Jankovsky, R. 2001. High Voltage SPT Performance. *36th Joint Propulsion Conference and Exhibit*, AIAA 2001-3774.
[22] Absalamov, S.K., Andreev, V.B., Colbert, T., Day, M., Egorov, V.V., Gnizdor, R.U., Kaufman, H., Kim, V., Korakin, A.I., Kozubsky, K.N., Kudravzev, S.S., Lebedev, U.V., Popov, G.A., Zhurin, V.V. 1992. Measurement of plasma parameters in the stationary plasma thruster (SPT-100) plume and its effect on spacecraft components. *44th AIAA/ASME/SAE/ASEE Joint Propulsion Conference & Exhibit*, AIAA 2011-5809.